Research

Reduced spiking in entorhinal cortex during the delay period of a cued spatial response task

Kishan Gupta[1], Lauren A. Keller, and Michael E. Hasselmo

Center for Memory and Brain, Department of Psychology, Graduate Program for Neuroscience, Boston University, Boston, Massachusetts 02215, USA

Intrinsic persistent spiking mechanisms in medial entorhinal cortex (mEC) neurons may play a role in active maintenance of working memory. However, electrophysiological studies of rat mEC units have primarily focused on spatial modulation. We sought evidence of differential spike rates in the mEC in rats trained on a T-maze, cued spatial delayed response task. Animals begin at the base of the T-maze where a 1-sec white noise and visual light cue are presented on the left or right side of the maze. Rats are rewarded for responding toward the cued direction. In correct trials, we observed decreased spike rates during the delay period, the time interval between cue presentation and reward delivery. Firing-rate histograms show significant decreases during the delay period compared to 5-sec windows from both pre-cue and post-reward periods. We analyzed how running speed and trajectory specificity correlated to spike rate. Twice as many cells were responsive to cue alone compared to running speed. Trajectory specificity did not relate significantly to firing rate. Decreased spike rate may reflect active maintenance in other structures inhibiting mEC. Alternately, the reduction may reflect decreases in background activity during enhanced attention and cholinergic modulation. Lastly, animals often ran through the T-maze choice-point with varying speed. We calculated the spatial posterior probability density from spike rates during these choice-point passes. Slow passes through the choice point were characterized by greater probability of decoding to the reward locations on correct trials compared to quick passes on the maze consistent with similar "look-ahead" properties previously reported in the hippocampus and ventral striatum.

[Supplemental material is available for this article.]

Multiple memory systems play a role in decision-making mechanisms in animals performing behavioral tasks. Of these systems, working memory provides a temporary store for information during performance of cognitive tasks (Baddeley and Wilson 2002; Hasselmo and Stern 2006). Previous studies in animals suggest that localized networks in the prefrontal cortex perform active maintenance of neural activity representing familiar stimuli in delayed-match-to-sample tasks (Fuster 1973), cued-choice behavior (Fujisawa et al. 2008), and object recognition (Asaad et al. 1998). However, parahippocampal structures have also been implicated as a buffer for working memory in rodents and primates (Hasselmo and Stern 2006). Unit recording has demonstrated entorhinal neurons that fire during the delay period of delayed-match-to-sample tasks in rats (Young et al. 1997) and monkeys (Suzuki et al. 1997).

Intracellular recording from in vitro slice preparations of rat medial entorhinal cortex (mEC) demonstrates neurons that persistently spike after a single depolarization during pharmacological activation of acetylcholine receptors (Klink and Alonso 1997; Egorov et al. 2002; Yoshida et al. 2008). Several computational models have demonstrated how these intrinsic mechanisms for persistent spiking activity could provide a mechanism for maintenance of working memory for novel inputs during delayed-match-to-sample (DMS) tasks (Lisman and Idiart 1995; Jensen and Lisman 1996; Fransén et al. 2002; Koene et al. 2003).

Based on slice experiments and computational modeling, we might expect to see an elevation in mEC activity after cue presentation that parallels the persistent spiking observed after a single depolarizing current injection in slice preparations. Periods of elevated spiking have been observed during spatial alternation by rats on T-mazes where elevated spike rates in the stem of the maze can differentially precede a leftward turn or a rightward turn (Lipton et al. 2007). For other behavioral variables, mEC differential spiking is notable for spatial cell types like grid cells that have location-specific firing rates (Hafting et al. 2005; Barry et al. 2007; Moser and Moser 2008; Brandon et al. 2011) and for cells that respond on the basis of head direction (Sargolini et al. 2006; Brandon et al. 2012). We sought evidence of differential spike rates in the mEC in rats when presented with an auditory and visual cue paired with a specific turning response for reward on a T-maze.

Previous work has also found neural ensembles in the rat hippocampus (Johnson and Redish 2007) and ventral striatum (van der Meer and Redish 2009, 2010) that exhibit nonlocal representations as rats pass through critical choice points on T-maze tasks. Such ensemble activity may be part of larger cognitive processes including trajectory planning (Ferbinteanu and Shapiro 2003; Jensen and Lisman 2005) and reward expectation (van der Meer and Redish 2009). In addition to looking for evidence of differential spiking associated with cued behavior, our study also tested for nonlocal representations of mEC neural ensembles.

Results

Behavior

All animals ($n = 3$) were pretrained on the cued spatial delayed response task (Fig. 1A) prior to testing, which typically allowed them to start above chance (chance = 50%) on testing session 1. Over the course of 24 testing sessions (see Fig. 1B), mean accuracy gradually increased from a minimum of 60% to a maximum

[1]**Corresponding author.**
E-mail kishang@bu.edu.
Article is online at http://www.learnmem.org/cgi/doi/10.1101/lm.025866.112.

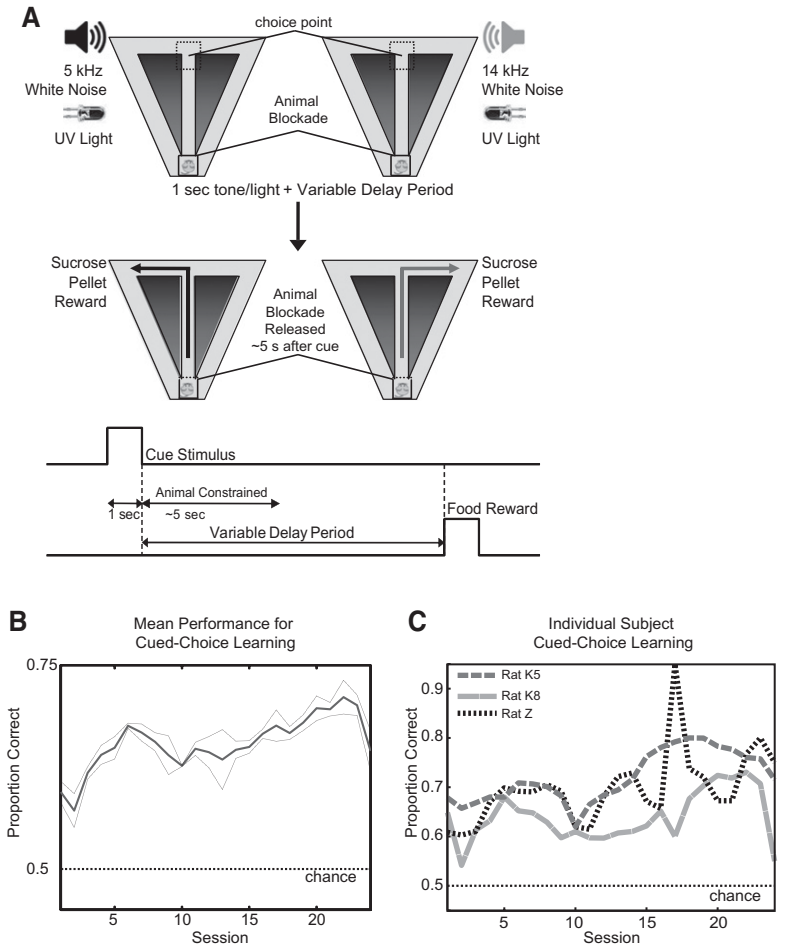

Figure 1. (*A*) Each trial starts with the rat held at the base of the stem with a blockade. At this time, a 1-sec cue stimulus is delivered, consisting of filtered white noise with a frequency cut-off of either 5 kHz or 14 kHz. A UV light is activated above the correct reward location (visible over the blockade). After a 4- to 6-sec period, the blockade is removed. The rat moves up the stem and makes a choice to turn into either the left (correct after 5 kHz) or right reward arm (correct after 14 kHz). If the correct choice is made, the rat receives two sucrose pellet rewards at the end of the reward arm. The rat returns on the diagonal return arms to the base of the stem for the next trial. (*B*) Mean learning performance by all subjects over 24 sessions with 95% confidence intervals. (*C*) Individual subject learning performance over 24 sessions.

of 71%, similar to previously studied auditory-cued choice tasks on T-mazes in rats (Johnson and Redish 2007). Each rat made significantly more correct turns than chance, as shown in Figure 1C ($P < 0.05$, binomial test). Rats were able to reach a maximum of 95% performance during training sessions and >80% on some testing sessions. As rats were pretrained prior to surgery, they gradually improved to their peak performances, with each rat performing at approximately the same degree.

Cell types

Of the 869 cells recorded, 529 individual cells were stably recorded on the T-maze and open-field environments. Spatial cell types included grid cells ($n = 58/529$, 11% of cells) (Fig. 2A), head direction (HD) cells ($n = 95/529$, 18% of cells) (Fig. 2B), and unclassified spatially modulated cells ($n = 74/529$, 14% of cells) (Fig. 2C). The latter group may include putative boundary vector cells (O'Keefe and Burgess 1996; Barry et al. 2006; Solstad et al. 2008), grid cells with very large spacing, and other nongrid spatial cell types. Grid cells on the T-maze typically had multiple firing fields similar to place cells on a T-maze, and their firing fields were sometimes shifted relative to their location in the open field. Head direction cells typically retained their orientation on the T-maze compared to the open field, apparently fixing to global environmental cues. Remaining cell types were characterized as interneurons ($n = 12/529$, 2% of cells) or nonspatial principal neurons ($n = 290/529$, 55% of cells) and exhibited no significant spatial correlate in the open field or T-maze. Principal nonspatial cells were recorded in layers V, III, and II. The majority of grid cell recordings appear to come from layer V, concomitant with HD cells and unclassified spatially modulated cells, and layer II. Lesion sites in the mEC show final recording sites predominantly in layers II and III (Fig. 3).

Spike raster

We recorded 869 unique cells localized in the medial entorhinal cortex identified by cluster cutting the data accumulated from three rats (for cluster cutting examples, see Supplemental Figs. S1, S2). T-maze sessions where tetrodes were not turned from the previous session were recorded but not included in the final count. In contrast to our initial hypothesis of increased spiking during the delay period, rastergrams with temporal alignment at cue onset showed decreases in cumulative spike counts after cue presentation in all animals (see Fig. 4). For all recorded cells, 19% (95% confidence interval: [16%, 22%]) showed a significant difference in spike rate ($P < 0.05$, two-tail Student's *t*-test with Holm-Bonferroni correction) from the pre-cue interval to the delay period. Compared to the post-reward interval, delay period spike rate was significantly suppressed in 29% of cells ($P < 0.05$, two-tail Student's *t*-test with Holm-Bonferroni correction, 95% confidence interval: [26%, 32%]). In 91% of the cells (95% confidence interval: [89%, 93%]), the pre-cue interval spike rate did not vary significantly ($P > 0.05$, two-tail Student's *t*-test with Holm-Bonferroni correction) from their post-reward interval spike rate (Fig. 5). Breaking the data up by cell type, similar proportions of cells are significant ($P < 0.05$, two-tail Student's *t*-test with Holm-Bonferroni correction) for the three interval-comparisons. Nonspatial principal cells (NP), grid cells (GC), head direction cells (HD), unclassified spatially modulated (SM), and interneurons (IN) each demonstrated the following respective significant proportions for each given comparison:

Pre-cue to delay period: NP, 18%; GC, 15%; HD, 18%; SM, 31%; IN, 17%.
Delay period to post-reward: NP, 27%; GC, 26%; HD, 24%; SM, 24%; IN, 42%.
Post-cue to post-reward: NP, 10%; GC, 9%; HD, 9%; SM, 8%; IN, 17%.

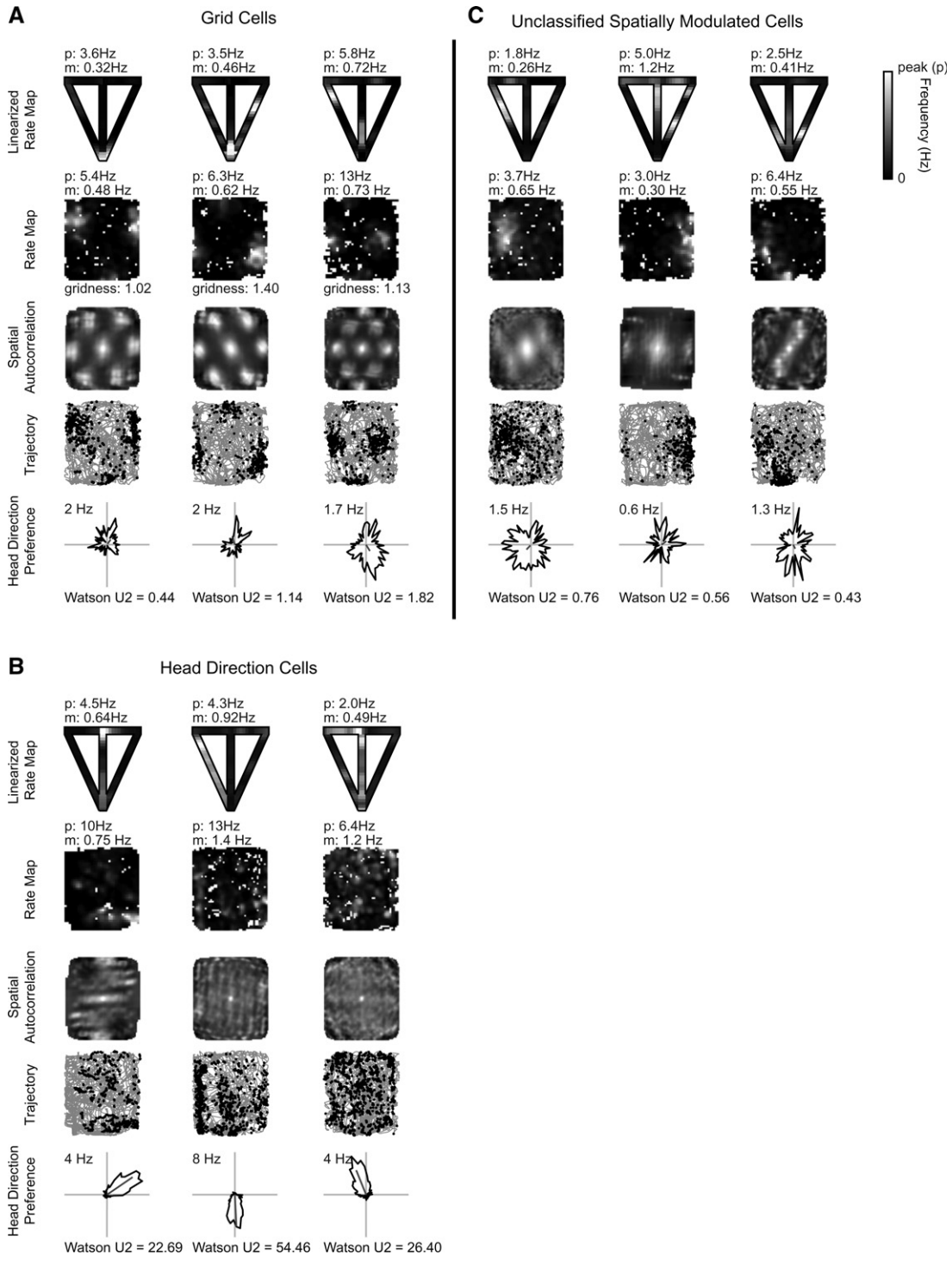

Figure 2. Examples of spatial cells recorded on the T-maze and open field. Panels *A*, *B*, and *C* show three grid cells, three head direction cells, and three spatially nonselective cells, respectively. T-maze recording (panel row *1*): reconstructed T-maze rate map from linearized position with mean (m) and peak (p) firing rate shown. Open-field recording (rows *2*–*5*): mean (m) and peak (p) firing rate shown *above* the rate map (panel row *2*); spatial autocorrelation with gridness score for grid cells only (panel row *3*); trajectory (gray line) of rat with spike locations (black dot) overlaid (panel row *4*); and polar rate map showing head direction preference with maximum firing rate *above* and Watson U2 score *below* (panel row *5*).

Unclassified spatially modulated cells had a larger proportion of cells significant for a spike-rate reduction compared to other cell types for the pre-cue–delay period comparison ($P = 0.0065$, $\chi^2[1] = 7.4$). However, other interval comparisons for this cell type do not contrast with the population statistics (delay period–post-reward: $P = 0.6809$, $\chi^2[1] = 0.17$; pre-cue–post-reward: $P = 0.6300$, $\chi^2[1] = 0.23$). Interneurons varied from the population proportions for delay period–post-reward and post-cue–

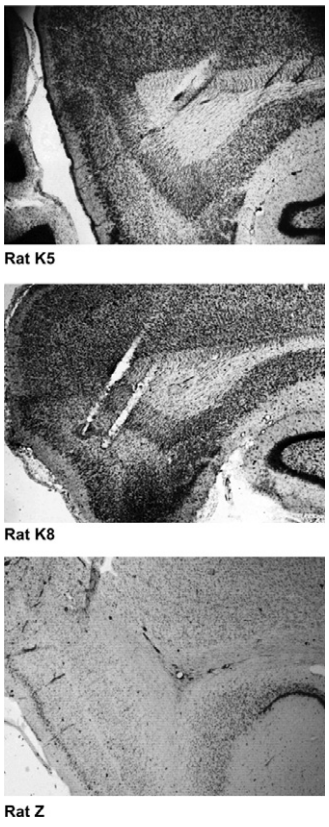

Figure 3. Histology. Nissl-stained sagittal sections for all three rats. Tetrode tracks are evident through layers II–V of medial entorhinal cortex.

post-reward interval comparisons. However, the differences for this cell category are based on 12 recorded interneurons and are subject to undersampling.

Spike-rate covariates

Temporally aligned plots of mean running speed plotted against the cumulative raster suggested speed as a possible covariate for predicting action potentials in several cells (Fig. 4). Care was taken to limit a rat's motion during and after the cue for approximately 4–6 sec to see if suppression effects occurred during stationary periods (see Materials and Methods). Representative examples of mean running speed are shown in Figure 4, where it is clear that, during stationary periods after cue presentation, animal subjects still had decreased cumulative spike counts relative to the pre-cue interval. Quantifying the effect of speed vs. the effect of cue, we ran a linear regression model predicting spike rate from standardized Z-score measures of speed and temporal proximity from the most recent cue, controlling for spatial location and head direction preference for spatial cell types (see Materials and Methods). Thirty-one percent of cells had a significant covariate ($P < 0.05$, two-tail Student's *t*-test) of cue alone compared to 17% of cells significant for speed alone (Fig. 6A). In addition, 17% displayed significance for both covariates. Within this smaller population, an effect size ratio relating the effects of cue to speed showed a median effect size ratio of 1.33, indicating a relatively larger effect from cue than from speed (Fig. 6B). Overall, nearly twice as many cells had a significant effect from cue alone, and those cells with responses to cue and speed had a larger median effect from cue.

Trajectory-specific firing

For all $n = 529$ cells stably recorded in both the open-field and T-maze environments, 10 cells had a significant covariate in right- or left-reward-bound trajectory for firing rate along the stem (two-way ANOVA grouped by turn and T-maze sector). Supplemental Figure 3 shows the left and right trajectories with action potentials from each of these cells. All the plots show very low occupancy-normalized firing rates (<1.5 Hz) in any given stem sector for a right- or left-reward-bound turn. Because of the low firing rates along the stem, it is possible these cells are aberrantly significant. Overall, there does not appear to be widespread trajectory-specific firing.

Ensemble decoding

The Bayesian decoding method employed here gives the probability distribution of any metric gathered during recording as a function of the number of spikes in specific selected recording windows. In the data shown in Figure 7, left and right correct laps have been pooled together. The overall decoding shows that the decoded position usually reflects actual position (dark diagonal band of high values in Fig. 7A), but there is a darker horizontal band of decoded activity for the feeder location that appears when the rat is at a variety of actual positions in the task, suggesting that the neural circuits contain activity associated with the feeder location at other locations such as the choice point (rat is presumably "thinking about" the feeder). There are also darker bands throughout the task associated with the cue and choice point.

Figure 7B shows the decoding analysis for long passes (time spent at choice point > 2.5 sec) vs. short passes (time spent at choice point < 1 sec). During long passes, there is an elevated probability of decoding to the feeder, p(Feeder), compared to decoding to the feeder during short passes (two-way ANOVA, $F_{(1,2222)} = 123.3$, $P < 10^{-10}$). Also, the probability of decoding tracks movement through the choice point. P(Feeder) was elevated significantly with the choice-point and post-choice-point locations (two-way ANOVA, $F_{(2,2222)} = 31.5$, $P < 10^{-10}$). In Figure 7C, p(Feeder) ratio measures the average probability of decoding to the feeder normalized by the pre-choice-point epoch, showing increased p(Feeder) for long passes and for the choice-point and post-choice-point regions.

We found decoding associated with future reward location when we repeated the above analysis without pooling the data, categorizing each decoding epoch by correct and incorrect laps given the type of cue presented. Figure 8A shows eight separate panels varied by short pass or long pass through the choice point and using correct laps or incorrect laps for decoding epochs. As with the pooled analysis, during long passes, when the animal spends more time at the choice point for a given left- or right-associated cue, there is elevated probability decoding to a feeder compared to short passes (5-way ANOVA, $F_{(1,5456)} = 50.6$, $P < 10^{-10}$). If animals make a short pass through the choice point, decoding to the appropriate feeder location (e.g., left feeder given left cue) is not significantly different between error and correct trial decoding epochs (left feeder: $P = 0.9514$, right feeder: $P = 0.1448$, two-tail Student's *t*-test with Holm-Bonferroni correction). However, animals making a long pass through the choice point decode with greater probability to the correct feeder during correct trials compared to error trials (left feeder: $P < 10^{-6}$, right feeder: $P < 10^{-5}$, two-tail Student's *t*-test with Holm-Bonferroni correction). This can be seen in Figure 8A as a darker band at the left feeder for correct left cue responses (top left), and a darker band at the right feeder for correct right cue responses (bottom left). Figure 8B shows these relationships with p(Feeder) ratios normalized by the mean decoding probability of the pre-choice-point epoch.

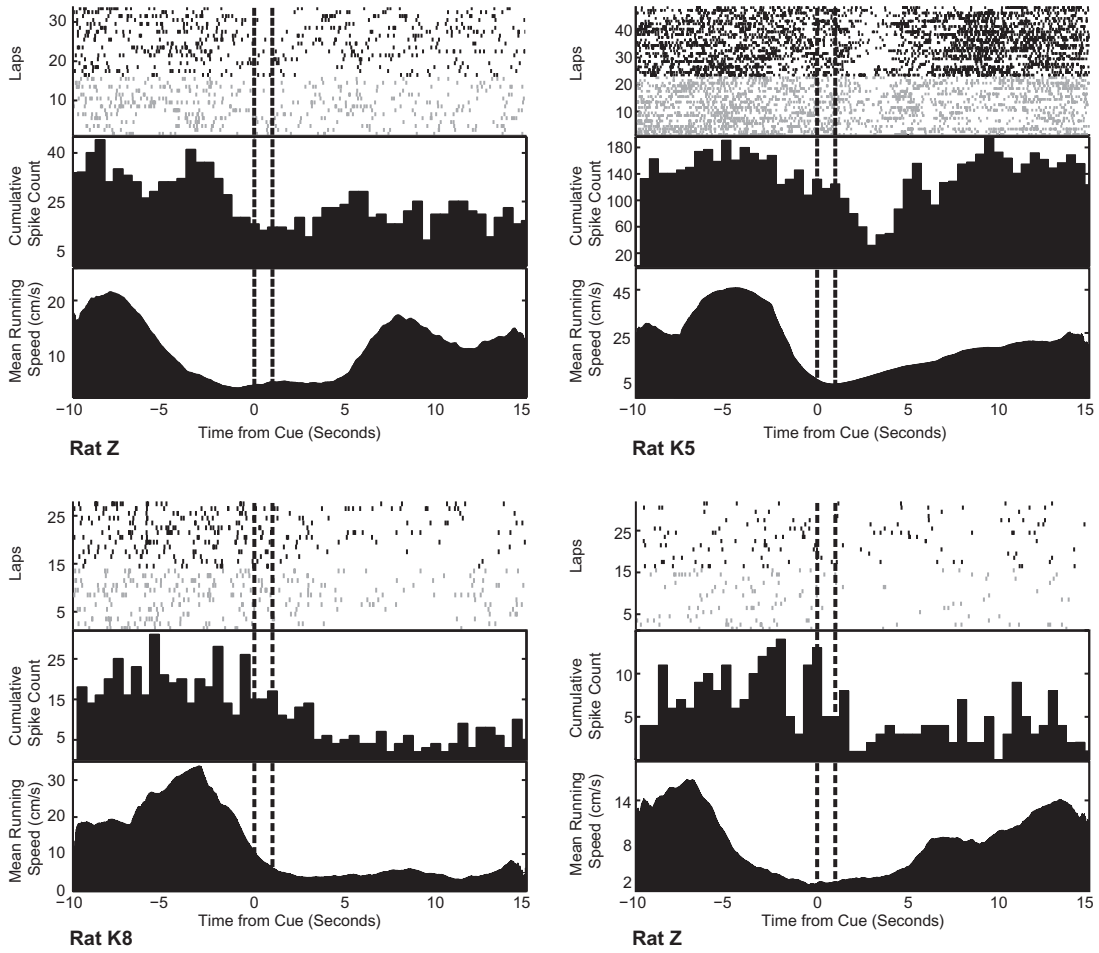

Figure 4. Four separate rastergram panels from a representative cell for each animal on a single session. Each rastergram panel includes: (*top*) sample raster plots for each correct right (black) or left (gray) turn lap temporally aligned to the 1-sec cue presentation (vertical dash interval); (*middle*) cumulative spike frequency histogram in 0.5-sec bins; (*bottom*) mean running speed at each time interval over laps (cm/sec).

In Figure 8A, the probability of decoding to an inappropriate reward site (e.g., right feeder given a left cue) is significantly higher for long passes through the choice point using error trials vs. correct trials for decoding epochs (left feeder: $P < 10^{-10}$, right feeder: $P < 10^{-10}$, two-tail Student's *t*-test with Holm-Bonferroni correction). This can be seen as more shading that is more uniform across left and right feeder locations for incorrect responses (right side of figure). If p(Feeder) is normalized by the mean probability from pre-choice-point decoding epochs where animals made long passes during correct trials, then it is clear that long passes from correct trials produce the lowest probability of decoding to the inappropriate feeder site compared to any other decoding epoch (Supplemental Fig. S4).

Discussion

The current experiment sought evidence of elevated spiking activity in the mEC of rats actively maintaining a representation of an auditory and visual cue during the delay period of an appetitive T-maze task. However, in contrast to the predicted difference, the data showed a reduction in firing rate after cue presentation from mEC neurons. This reduction of firing had strong modulation by cue timing compared to modulation by the animal's running speed. In addition, observed firing rates of all mEC neurons, including grid cells, did not vary significantly with a left- or right-reward-bound trajectory. Behaviorally, we observed animals move quickly or slowly through the choice point. The decoding analysis suggested that, at longer, slower passes through the choice point, mEC neural ensembles decoded to the feeder location with significantly higher probability than when the animal made shorter, quicker passes. These findings are discussed further below.

Post-cue reduction in firing rate

We originally hypothesized the mEC would demonstrate elevated persistent spiking after cue presentation corresponding to single-neuron behavior in vitro when a neuron injected with a depolarizing current stimulus shows persistent spiking after the depolarization (Klink and Alonso 1997; Egorov et al. 2002; Yoshida et al. 2008). However, we did not observe such persistent firing in any neurons recorded from the mEC including spatial subtypes. This may be due to differences in modulatory influences on neurons during recording. Pharmacological manipulations within the mEC have focused on increasing or decreasing acetylcholine (ACh) levels (Klink and Alonso 1997; Egorov et al. 2002; Yoshida et al. 2008), which change in response to novelty (Acquas et al. 1996; Parikh et al. 2007). Consistent with the proposed role of cholinergic modulation of cellular intrinsic persistent spiking,

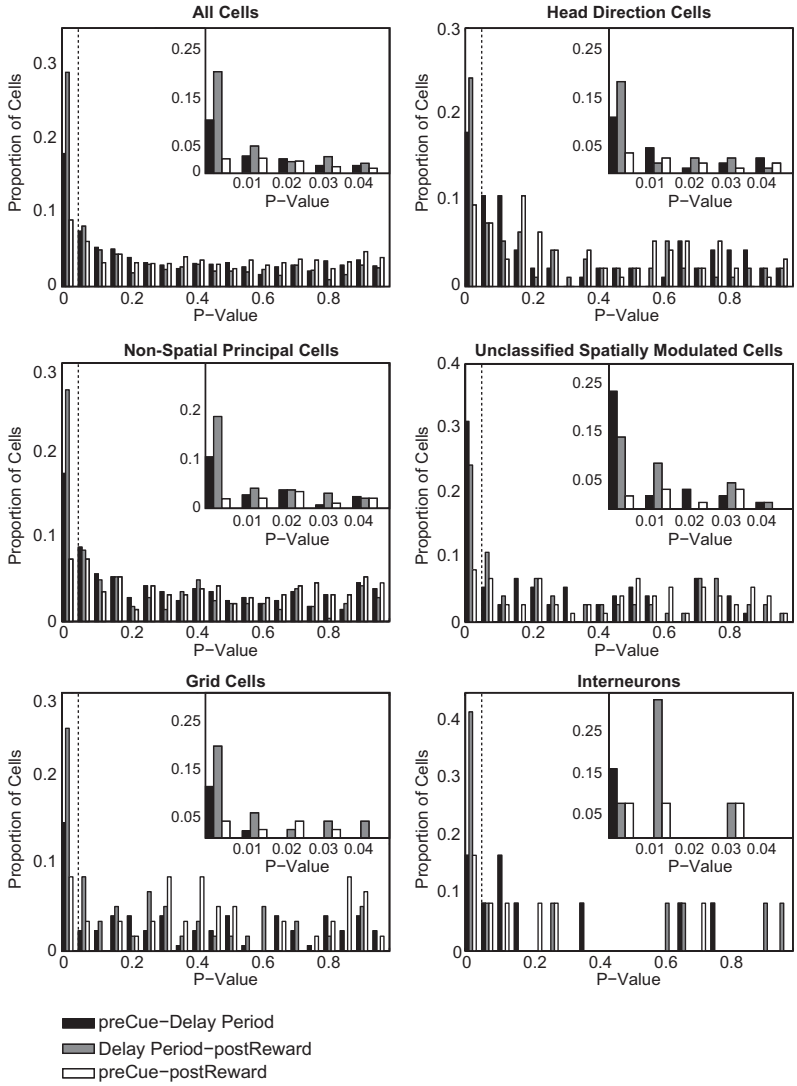

Figure 5. Histograms of *P*-values for three comparisons in spike rate for all recorded neurons and for spatial and nonspatial subtypes from all three rats. The *insets* show the data for $P < 0.05$ in smaller bin sizes. See Materials and Methods for interval definitions. (Black) Two-tail *t*-test of the elevated spike-rate distribution 5-sec pre-cue interval compared to delay period, (gray) two-tail *t*-test of elevated spike-rate distribution 5-sec post-reward interval compared to delay period, (white) two-tail *t*-test of spike-rate distribution differences between 5-sec pre-cue and 5-sec post-reward intervals. All *t*-tests are corrected for multiple comparisons using the Holm-Bonferroni method.

cholinergic modulation appears to be important for working memory tasks. Cholinergic deafferentation in the entorhinal cortex impairs performance in rats presented with novel stimuli in a delayed-nonmatch-to-sample (DNMS) task (McGaughy et al. 2005). Infusions of scopolamine impaired the encoding of trace fear conditioning in rats (Bang and Brown 2009), and such impairments have been shown to be dose-dependent with the M1-antagonist pirenzepine (Esclassan et al. 2009). In human functional magnetic resonance imaging (fMRI) studies, the hippocampus and parahippocampal regions show elevated activity for novel stimuli compared to familiar stimuli (Stern et al. 2001; Schon et al. 2004, 2008) and correlations of delay period activity with subsequent memory that are reduced after scopolamine is administered to subjects (Schon et al. 2005).

The key feature distinguishing our study and these previous studies may stem from stimulus novelty. As our rats were overtrained by the time testing began, the task was familiar to the animals. It is possible that acetylcholine levels were not elevated enough for persistent mEC activity. Because all mEC cell types show roughly equivalent cue-evoked suppression, a structure external to the mEC may induce this effect. The prefrontal cortex (PFC) has elevated activity after cue presentation in similar tasks where the animal has become familiar with stimuli (Fuster 1973; Baeg et al. 2003; Di Pietro et al. 2004; Fujisawa et al. 2008). The PFC's role in working memory for familiar stimuli makes it a candidate region to perform simultaneous mEC and PFC recordings.

Cue-evoked effect

We sought to rule out the possibility that the reduction in firing rate could also have been correlated not only to the cue, but to other covariates such as running speed and trajectory-specificity. Running speed correlates with mEC activity, particularly with grid, conjunctive grid, and head direction cells (McNaughton et al. 1983; Quirk et al. 1992; Sharp 1996; O'Keefe et al. 1998; Sargolini et al. 2006). Our results show twice as many cells responsive to the cue as to running speed. Those cells responsive to both covariates had larger effect size from the cue (Fig. 6B). Though the mEC firing rate was suppressed during the delay, mEC activity did respond to nongeometric aspects of the environment, particularly the task demands of attending to and interpreting the cue.

Because of previous studies on differential activity based on running trajectory (Frank et al. 2000; Wood et al. 2000; Ferbinteanu and Shapiro 2003; Lipton et al. 2007), we looked at whether the mEC in this instance would also have similar differential behavior. Only 10 cells had a significant correlation with a left or right turn toward reward (Supplemental Fig. S3). However, these cells exhibited relatively low, near zero firing rates along the T-maze stem, and any statistical significance is likely an aberration from too few spikes. The overall lack of trajectory disambiguation seen here is not inconsistent with the small population percentage of dorsocaudal mEC (dcMEC) neurons selective for trajectory in Lipton et al. (2007). This issue of low firing rates in some cells was proposed by Lipton et al. (2007) as an explanation for their nonoverlapping results from the two statistical techniques (ANOVA and log-likelihood modeling) they employed to identify cells selective for trajectory.

Other differences between our result and other disambiguation studies might be attributed to the difference between the cued behavioral task we employ and the spatial alternation tasks employed in the previous studies. In our task, a pseudorandom presentation of light and noise cue is the dominant task stimulus for the animal to obtain reward. In spatial alternation,

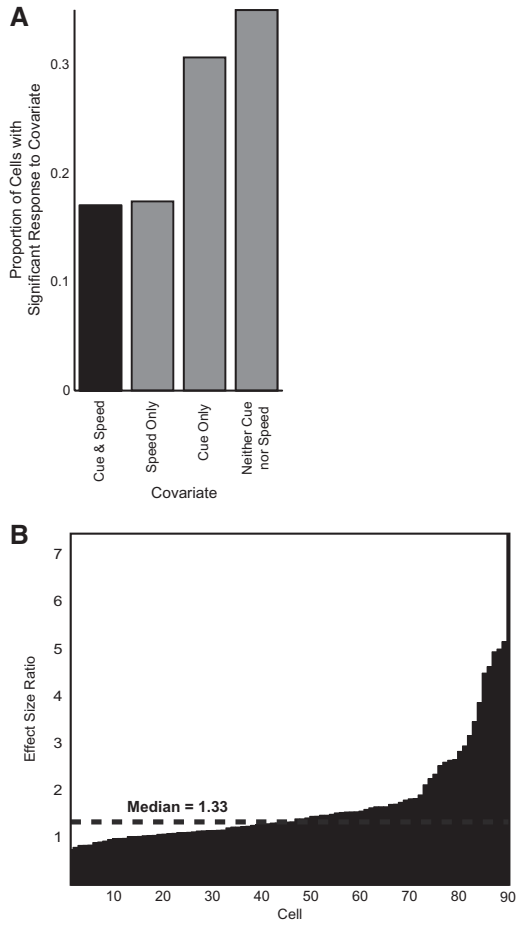

Figure 6. Effect size ratio. (*A*) Proportion of cells with significant effects from both cue and speed (17%), speed alone (17%), cue alone (31%), and no effect from either covariate (34%). The black column—the proportion of cells with significant response to both cue and speed—is the sample used for analysis in panel *B*. (*B*) Linear regression effect size (see Materials and Methods) of cue to speed on neuron spike rate for all cells with significant effect from both cue and speed.

remembering the previous reward location and the path taken is the most salient stimulus to obtain reward.

In addition, our task has a delay, which further adds complexity vs. nondelayed versions of continuous spatial alternation. In one study, where delayed continuous spatial alternation was performed, place cells in region CA1 of the hippocampus showed reduced trajectory encoding during the delayed version of the task (Ainge et al. 2007). The introduction of delay distinguishes spatial alternation behavior from context-dependencies that subsume previous spiking characteristics seen in neurons recorded as animals perform continuous spatial alternation. In our task, a similar effect could be occurring in the mEC where introducing a delay after cue presentation changes the mEC's role of trajectory encoding along the stem. This role could be assumed by other structures and/or generated by other underlying mechanisms as suggested for the hippocampus by Ainge et al. (2007).

Encoding reward location

Animals exhibited short (brief) and long (slow) passes through the choice point. During long passes, the animal often paused, exhibiting head movements associated with vicarious trial and error

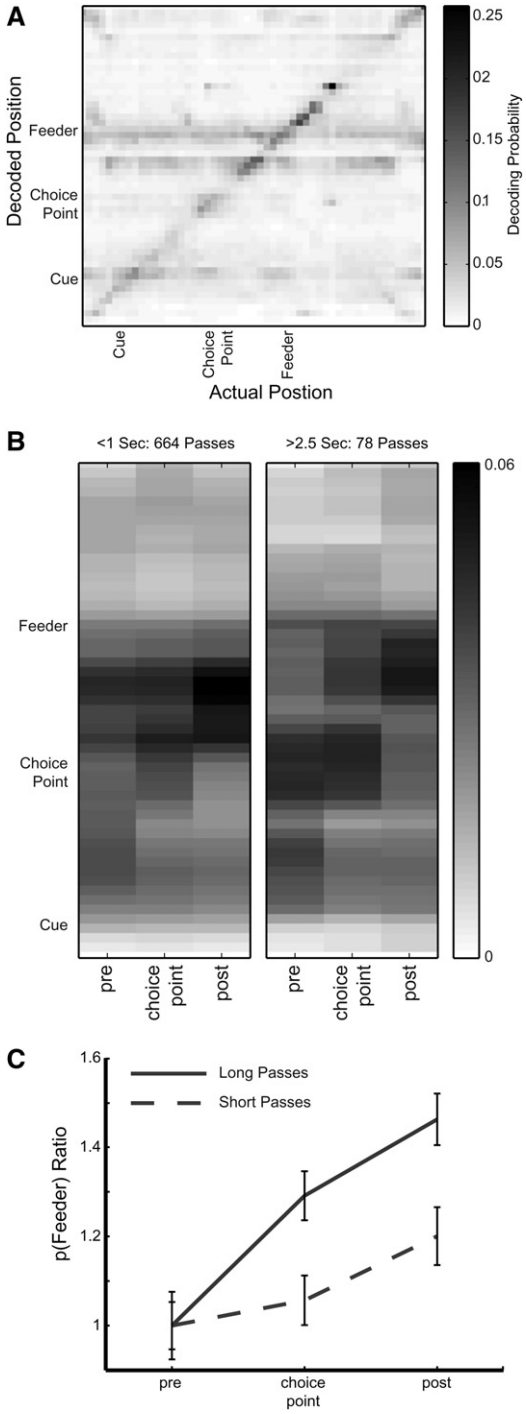

Figure 7. Decoding of entorhinal ensembles. (*A*) Average posterior spatial probability of yielding decoded position from spike data gathered over the given actual position. For any given actual position, the most probable decoded position tends to be the actual position itself, near cue presentation, and just before and after passing through the feeder. (*B*) Posterior probability distributions for short (*left* panel) and long (*right* panel) passes through the choice point. Pre- and post-choice-point epochs are 1-sec intervals to and from the choice point, respectively. The progression of elevated decoding probability tracks the animal as it runs through the choice point. The average probability of decoding to the feeder location is higher in long passes compared to shorter passes. (*C*) Average feeder decoding probability is normalized to pre-choice-point levels, showing long passes highly significant during the choice-point and post-choice-point intervals ($P < 10^{-10}$, $F = 123.01$).

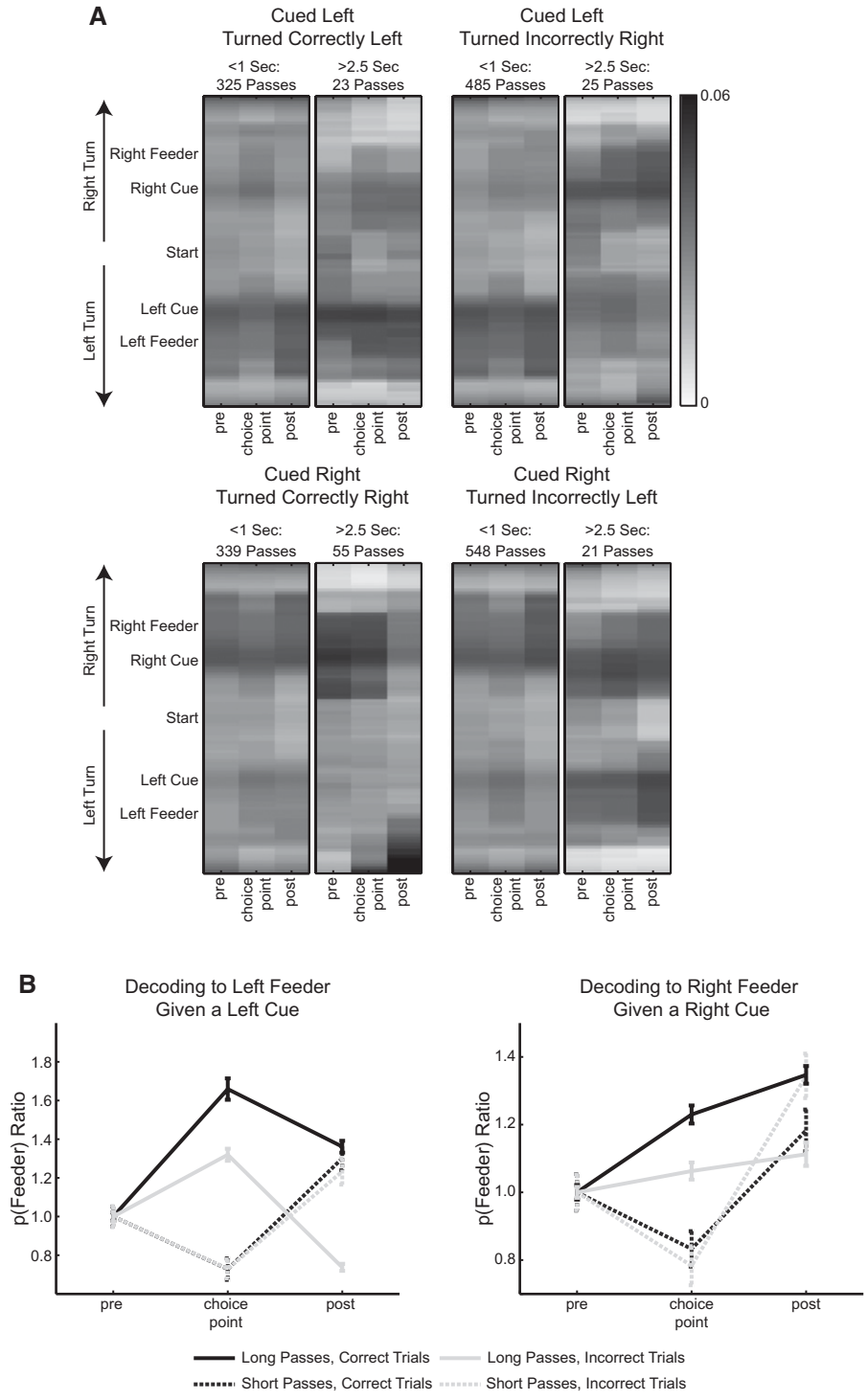

Figure 8. Decoding of entorhinal ensembles for both left and right turns on correct and error trials. (*A*) Like Figure 7, these panels show posterior probability distributions for decoding to a positive (right turn) or negative (left turn) location on the T-maze. The eight panels are separated into short (time spent at choice point < 1 sec) or long (time spent at choice point > 2.5 sec) passes and whether the animal traversed correctly to the left, correctly to the right, incorrectly to the left, or incorrectly to the right. Note that in long passes before correct responses, the decoding shows greater activity for the correct feeder location. (*B*) Average feeder decoding probability normalized to pre-choice-point levels. For long passes, decoding to the correct feeder is higher during correct trials vs. error trials (left feeder: $P < 10^{-6}$, right feeder: $P < 10^{-5}$, two-tail Student's *t*-test with Holm-Bonferroni correction). For short passes, decoding to the correct feeder is not significantly different for correct and error trials (left feeder: $P = 0.9514$, right feeder: $P = 0.1448$, two-tail Student's *t*-test with Holm-Bonferroni correction).

(VTE) (Johnson and Redish 2007; van der Meer and Redish 2010). Animals swiftly move to reward during short passes, but long passes allow more time for decision-making and possible expectations of reward outcome. The decoding analyses (Figs. 7, 8; Supplemental Fig. S4) indicate that mEC neural ensembles are encoding prospective reward locations during long passes compared to short passes through the choice point. Decoding from epochs where the animal makes a short pass through the choice point suggests that neural ensembles are not differentially encoding error trials from correct trials. However, during long passes, decoding epochs from correct trials shows that neural ensembles are encoding the correct feeder location for the given cue (Fig. 8A,B). Thus, on correct trials, decoding is stronger for the right feeder location after a right cue and stronger for the left feeder location after a left cue (Fig. 8A). When animals perform an error trial, decoding long passes from these epochs shows a concomitant increase in encoding the opposite, incorrect feeder location for the given cue. The mEC, like the ventral striatum (van der Meer and Redish 2009) and region CA3 of the hippocampus (Johnson and Redish 2007), may perform "look-ahead" activity toward locations of consequence such as reward. This behavior may also demonstrate forward sweeps, as seen in region CA3 of the hippocampus (Johnson and Redish 2007), but further fast-timescale analysis is necessary to accurately characterize this in the mEC. As noted in Ainge et al. (2012), in tasks where animals did not achieve automaticity or swiftness through a choice point, increased decision-making encoding for relevant future locations may be a feature of added task complexity.

In summary, the reduction in mEC spiking indicates network effects that dominate over intrinsic persistent spiking mechanisms manifested in slice preparations. The cellular mechanisms underlying persistent spiking in slice preparations may have a different manifestation in the awake-behaving animal.

Materials and Methods

Subjects

Three male Long-Evans rats, weighing between 400 and 500 g at the beginning of the experiment, served as subjects (Charles River Laboratories). Each animal was housed individually in plexiglass cages under a 24-h light/dark cycle with free access to water but food restricted to maintain approximately 85% ad libitum body weight. Animal habituation

to experimenters and testing environment took place at two different times—one week post-arrival from the vendor and one week post-surgery. All subjects were pre-exposed to an open-field (154 cm × 140 cm) with a white cue card affixed to a wall, where they were trained to forage for both Fruit Loop cereal (Kellogg Company) and sucrose precision pellets (Bio-Serv). Twenty-minute open-field sessions later served as controls for same-day T-maze recordings of both spatially and nonspatially modulated neurons.

Implant

Rats were implanted with a movable tetrode assembly consisting of 16 tetrodes, each insulated with 75-μm polyimide tubing (PolyMicro Technologies) inside 30-gauge steel cannulae (Small Parts, Inc.). Each tetrode, composed of four equal-length electrodes of 12-μm-diameter nichrome wire (Kanthal), is independently vertically driven, exiting the implant in a bundle with other channels encased in a 15-gauge steel cannula. The angle of the bundle with respect to the drive's vertical axis was about 25°.

Surgery

Subjects were given atropine (0.04 mg/kg) 20–30 min prior to induction of general anesthesia using inhalation of Isoflurane followed by injection of a ketamine cocktail (ketamine 12.92 mg/mL, acepromazine 0.1 mg/mL, xylazine 1.31 mg/mL). Upon demonstration of a blunted tail-pinch reflex, skin and cranial epithelium were removed. Ten to 12 skull screws were inserted along skull boundaries. Bone tissue was removed over the cerebellum where underlying dura was exposed to a single skull screw serving as an electrical ground. All screws were then covered with a thin layer of dental acrylic. The implant site grazes against the left bone ridge between parietal and postparietal skull bone (approximately AP −8.0, ML −4.6 from bregma). Craniotomy proceeded with subsequent dura removal, and upon lowering the implant bundle onto the brain, the implant was transiently secured with Kwik-Sil (World Precision Instruments), followed by several layers of dental acrylic. Ground screw wires were attached to the implant's electronic interface board (EIB), and any exposed wire was also covered in dental acrylic. Tetrodes were lowered into the brain at the bundle angle to a depth of 2.8 mm below the dorsal surface. Post-surgical pain management included 0.1 mL buprenorphine IP and 4 mL of children's ibuprofen PO. Each day for 4-d post-op, infection control was managed with cephalexin via water delivery at 168 mg/100 mL and daily cage changes for 7 d during animal recovery. All surgical procedures followed National Institute of Health guidelines and the protocol approved by the Boston University Institutional Animal Care and Use Committee.

Neural recordings

Animals were tested daily on an elevated T-maze and an open field during unit recordings. Post-recording, tetrodes were turned at least 35 μm and no more than 70 μm (van de Meer and Redish 2009) per day. The tetrodes were connected to analog unit gain preamplifiers on the head stage. Recorded signals were linked via the head stage to digital amplifiers augmenting the signal 5000–20,000 times. All signals were sampled at 32.556 kHz and digitally bandpass-filtered from 1 Hz to 2 kHz by the 64-channel Cheetah Digital Lynx acquisition system (Neuralynx Corp.). Units crossing each electrode's threshold were recorded for offline cluster cutting. Position and head-direction data were calculated based on a green rostral diode and a red caudal diode video sampled at 30 Hz. Local field potential continuously sampled channels were referenced to the animal's ground or a reference cortical electrode (the reference electrode was chosen to have no apparent θ-modulated signal that would interfere with θ detection at the recording site).

Histology

Tetrodes were not moved after the final recording session. Tetrode positions were confirmed by passing 25-μA current for 20 sec though each tetrode one day prior to perfusion, creating a lesion visible after Nissl staining (Komorowski et al. 2009). Animals were overdosed with Isoflurane and were perfused intracardially with saline followed by 4% formaldehyde. Brains were extracted and were stored in 4% formaldehyde at 6°C at least 24 h. Seventy-two hours prior to slicing, brains were transferred into a 30% sucrose solution. The brain was sectioned along a sagittal plane (to visualize tetrode tracks) into 35-μm slices. Sections were mounted on glass slides and stained with a neutral red Nissl stain. All tetrode tip lesions were confirmed to be localized within the medial entorhinal cortex, as shown in Figure 3.

Cued spatial delayed response task

The rats performed the task on a T-maze with a stem length of 103 cm and a width across both reward arms of 115 cm and a track width of 10 cm. Diagonal return arms allowed rats to run from the reward sites at the end of each reward arm to the base of the stem. A sucrose precision pellet dropper (Med-Associates) delivering two 45-mg pellets (Bio-Serv) for correct turns was attached at each reward site. For a given cue and correct turn, only one dispenser was operational. Cue and reward delivery was manually controlled via scripts written in Matlab R2009B (Mathworks) with each output time-stamped to the Neuralynx Digital Acquisition System. The experimenter always stood behind the base of the stem of the T-maze.

Animals were pretrained prior to surgery for 1–2 wk in two 1-hr sessions daily on the T-maze in darkness. A 1-sec presentation of lateralized ultraviolet (UV) light and bandpass-filtered white noise at 5 or 14 kHz frequency was paired with left or right sucrose pellet reward, respectively (Fig. 1A). Initially, cue presentation occurred at the choice point of the T-maze with almost immediate pellet reward. Over the course of training, cue presentation was shifted to times when the rat was farther back along the center stem of the maze until the rat could adequately seek reward without distraction from near the base of the T-maze. During each session on pretraining days 1–5, a sequence of 35 rightward cues were presented, followed by a sequence of 35 leftward cues, while blocking the opposite half of the maze. After these initial pairings, the sequence of cues was presented in pseudorandom order to produce an equal presentation of left and right reward for every 20 trials (Johnson and Redish 2007). Animals were blocked at the base of the T-maze stem during and after cue presentation, for approximately 4–6 sec. For two animals, wooden peg blockades 9.5-cm wide sat inside the stem track, inhibiting motion up the track. To keep rats as stationary as possible during cue presentation, we transitioned to a clear box with sliding doors (Med-AssociatesT) for the final rat, yielding more precise delay period control.

Data analysis methods

Cluster cutting and alignment across recording sessions

Single-units were cut manually "offline" after each recording session. Neurons were discriminated by peak amplitude and principal components measures for each waveform (Offline Sorter, Plexon). Units with biologically realistic interspike intervals and characteristic spike time autocorrelations were retained. Waveform stability across T-maze and open-field sessions was confirmed by consistent cluster position and waveform profile on each electrode comparison (see examples in Supplemental Figs. S1, S2).

Position, direction, and speed estimation

The head stage for the unit recording preamplifier has a rostral green light-emitting diode situated 12 cm from a caudal red diode. Animal position was calculated as the centroid of the lit tracking diodes with no other visible light present. Up to five lost samples

due to shadow effects or reflections near environment boundaries were replaced by linear interpolation and directional data. Head direction was calculated as the angle between the rostral and caudal diodes. Running speed was calculated as the difference between calculated positions over time. For rastergram plots, running speed was calculated across each lap on the T-maze and averaged with a boxcar smoothing window of 2 sec (Fig. 4).

Cell selection

We categorized each neuron as a "nonspatial principal cell," "head direction cell," "grid cell," "unclassified spatially modulated cell," or "interneuron." Examples of spiking activity of spatial cell types are shown in Figure 2. Neurons with a gridness score (gridness measure 3 from Brandon et al. 2011) greater than zero were considered grid cells. Neurons with negative gridness scores but with Watson U2 scores >5 were classified as head directions cells. Unclassified spatially modulated cells were defined as cells with spatial information content >0.5 with negative gridness scores (Brandon et al. 2011). Neurons with narrow spike waveforms and rapid after-hyperpolarization after each spike were visually identified and classified as putative interneurons. Neurons that did not meet any of the above criteria for classification were labeled nonspatial principal cells.

Spike–rate analysis

Laps were defined as intervals between times of cue presentations. Two sessions had two separate laps with aberrant cue signals, and data from those epochs were thrown out. Each lap was aligned temporally at the cue presentation. Cumulative rastergrams summed data across laps into 0.5-sec bins (Fig. 4).

Spike-rate comparisons were made across spike trains for each session looking at control intervals with respect to the time of cue (t_{cue}) and reward (t_{reward}) onset. Comparisons for elevated spike rate in the "pre-cue" interval ($[t_{cue} - 5$ sec, $t_{cue}]$) and "post-reward" interval ($[t_{reward}$, $t_{reward} + 5$ sec$]$) with respect to the delay period ($[t_{cue} + 1$ sec cue duration, $t_{reward}]$) were considered significant with $P < 0.05$ from a two-tail Student's *t*-test. A third comparison looked at differences in the pre-cue interval ($[t_{cue} - 5$ sec, $t_{cue}]$) and the post-reward interval ($[t_{reward}$, $t_{reward} + 5$ sec$]$) with significance at $P < 0.05$ from a two-tail Student's *t*-test (see Fig. 5). All *P*-values were subsequently corrected for multiple comparisons using the Holm-Bonferroni method.

Effect size ratio

Covariates contributing to spike rate include animal running speed ("speed") and temporal proximity to preceding cue presentation ("cue"). For grid cells, head direction cells, and unclassified spatially modulated cells, the model included additional covariates to control for confounding by spatial location ("position") and head direction preference ("heading"). Nonspatial principal cells and interneurons did not significantly depend on the latter predictors. Each covariate was included in a linear regression model for each cell. All model predictors were converted to Z-scores yielding standardized coefficients β_{speed}, β_{cue}, $\beta_{position}$, and $\beta_{heading}$. These coefficients were considered significant for $P <$ 0.05 (two-tail Student's *t*-test). For those cells with significant dependence on both cue and speed, an effect size ratio was calculated as $\beta_{cue}/\beta_{speed}$.

Linearization

The T-maze was linearized to a 261-cm track along each arm of the maze, beginning and ending at the base of the maze. Tracking positions acquired during maze running were all mapped to the nearest pixel of an idealized maze template of 1-cm^2 bins. For every session, the template was overlaid on the tracking data by identifying the peak in the two-dimensional cross correlation between the ideal track bitmap and the binary matrix representing bins visited by the animal during that session. Since the cross-correlation is only useful for detecting translations of the maze under the camera, the orientation and resolution of the session was indicated manually. This was necessary because two recording rooms were used and equipment was shifted. Boston University performed air exhaust ventilation replacement requiring a 4-mo shutdown of our main laboratory facility. In this period, we transitioned our recording setup to a temporary new facility. All neurons were analyzed within session. Neurons recorded from rats tested in different locations showed similar overall results.

The sign of the linear position was changed to match the direction of each lap (Huang et al. 2009). Left-reward-bound laps are indicated by negative linear position, and right-reward-bound laps are indicated by positive linear position (Supplemental Fig. S5A,B).

Trajectory–specific firing

Post-linearization, the stem of the T-maze was defined as 12–90 cm from the base of the maze (0 cm) where the rats moved relatively straight. The stem of the maze was divided into six, 13-cm sectors, similarly sized to previous studies (Wood et al. 2000; Lipton et al. 2007). Occupancy-normalized spike rates were calculated for each cell, T-maze sector, and direction-specific trajectory where animal running speed was greater than 2 cm/sec (Wood et al. 2000; Lipton et al. 2007). The cell population was reduced to those cells ($n = 529$) from the rat subjects for which good cluster stability was achieved on the open field. Subsequent two-way ANOVA analysis compared spike rate to covariates of right-reward- or left-reward-bound trajectories and sectors 1–6 of the T-maze stem for each cell. Those cells significant for the covariate of trajectory are isolated and presented in Supplemental Figure 3.

Ensemble decoding

We performed decoding analysis motivated by previous studies (van der Meer and Redish 2009) showing that, at the choice point of a task during long passes (often pauses accompanied by head movements known as vicarious trial and error), rats show neural activity associated with the future location of the food reward. We applied a probabilistic one-step Bayesian decoding method (Zhang et al. 1998; van der Meer and Redish 2009; Brandon et al. 2012), using all clusters with at least 25 spikes per session ($n = 869$) with at least eight simultaneously recorded cells (70/94 sessions). For every 0.5-sec time bin, we calculated the rat's posterior probability for any location x, given the total number of spikes N in the time bin, $P(x|N)$, for each neuron. We did not assume a uniform prior, but rather the empirical prior, $P(x)$ for calculating this distribution. Posterior probability as a function of actual position is the average probability over all the times that position was visited during a session.

For Figure 7, all linear positions were converted to positive coordinates, looking particularly at the cue region (0–15 cm), the choice-point region (95–105 cm), and the feeder region (155–160 cm) (see Supplemental Fig. 5A). For Figure 8 and Supplemental Figure 4, linear positions were kept as negative (leftward turns) or positive (rightward turns). Training epochs for the decoding algorithm included the first lap and every other lap correctly traversed. For Figures 7 and 8 (looking at correct trials), the remaining correct laps made up decoded epochs. The decoder was employed additionally on error trials in Figure 8, where all error laps were used as decoding epochs.

To see the effect of pausing at the choice point, we compared average posterior spatial probability at the choice point to a 1-sec interval pre- and post-choice point for long passes (>2.5 sec) and short passes (<1 sec) through the choice point. Choice-point passing time was derived from the number of continuously sampled time-stamps from when the rat first entered the choice-point region to when the animal exited. Probability of decoding to the feeder was tested via two-way ANOVA for length of choice-point passing time (long vs. short) and to pre- and post-choice-point intervals (Fig. 7B). Probability of decoding to the feeder for each interval was normalized to the pre-choice-point epoch (Fig. 7C). In

the unpooled analysis, probability of decoding to the feeder was tested via five-way ANOVA for length of choice-point passing time (long vs. short), pre- and post-choice-point intervals, cue type (left-reward-associated or right-reward-associated), feeder location (left feeder or right feeder), and trial type (correct or error). Pairwise comparisons of individual distributions were made with Student's *t*-tests correcting for multiple comparisons using the Holm-Bonferroni method.

Acknowledgments

We thank Andrew Bogaard for programming assistance, Tyler Ware and Nathan Beer for technical assistance, and Dr. Sung Eun Yang for helping construct environments. We thank Dr. Howard Eichenbaum, Dr. Eric A. Zilli, and other members of the Hasselmo laboratory for constructive comments on the manuscript. Finally, we thank Dr. Lisa M. Giocomo, Dr. Matthijs A.A. van der Meer, and Dr. Uri T. Eden for useful dialog on methods. This work was supported by the National Institute of Mental Health R01 MH61492, R01 MH60013, and the ONR MURI N00014-10-1-0936.

References

Acquas E, Wilson C, Fibiger HC. 1996. Conditioned and unconditioned stimuli increase frontal cortical and hippocampal acetylcholine release: Effects of novelty, habituation, and fear. *J Neurosci* **16:** 3089–3096.

Ainge JA, van der Meer MA, Langston RF, Wood ER. 2007. Exploring the role of context-dependent hippocampal activity in spatial alternation behavior. *Hippocampus* **17:** 988–1002.

Ainge JA, Tamosiunaite M, Worgotter F, Dudchenko PA. 2012. Hippocampal place cells encode intended destination, and not a discriminative stimulus, in a conditional T-maze task. *Hippocampus* **22:** 534–543.

Asaad WF, Rainer G, Miller EK. 1998. Neural activity in the primate prefrontal cortex during associative learning. *Neuron* **21:** 1399–1407.

Baddeley A, Wilson BA. 2002. Prose recall and amnesia: Implications for the structure of working memory. *Neuropsychologia* **40:** 1737–1743.

Baeg EH, Kim YB, Huh K, Mook-Jung I, Kim HT, Jung MW. 2003. Dynamics of population code for working memory in the prefrontal cortex. *Neuron* **40:** 177–188.

Bang SJ, Brown TH. 2009. Muscarinic receptors in perirhinal cortex control trace conditioning. *J Neurosci* **29:** 4346–4350.

Barry C, Lever C, Hayman R, Hartley T, Burton S, O'Keefe J, Jeffery K, Burgess N. 2006. The boundary vector cell model of place cell firing and spatial memory. *Rev Neurosci* **17:** 71–97.

Barry C, Hayman R, Burgess N, Jeffery KJ. 2007. Experience-dependent rescaling of entorhinal grids. *Nat Neurosci* **10:** 682–684.

Brandon MP, Bogaard AR, Libby CP, Connerney MA, Gupta K, Hasselmo ME. 2011. Reduction of theta rhythm dissociates grid cell spatial periodicity from directional tuning. *Science* **332:** 595–599.

Brandon MP, Bogaard AR, Andrews CM, Hasselmo ME. 2012. Head direction cells in the postsubiculum do not show replay of prior waking sequences during sleep. *Hippocampus* **22:** 604–618.

Di Pietro NC, Black YD, Green-Jordan K, Eichenbaum HB, Kantak KM. 2004. Complementary tasks to measure working memory in distinct prefrontal cortex subregions in rats. *Behav Neurosci* **118:** 1042–1051.

Egorov AV, Hamam BN, Fransen E, Hasselmo ME, Alonso AA. 2002. Graded persistent activity in entorhinal cortex neurons. *Nature* **420:** 173–178.

Esclassan F, Coutureau E, Di Scala G, Marchand AR. 2009. A cholinergic-dependent role for the entorhinal cortex in trace fear conditioning. *J Neurosci* **29:** 8087–8093.

Ferbinteanu J, Shapiro ML. 2003. Prospective and retrospective memory coding in the hippocampus. *Neuron* **40:** 1227–1239.

Frank LM, Brown EN, Wilson M. 2000. Trajectory encoding in the hippocampus and entorhinal cortex. *Neuron* **27:** 169–178.

Fransén E, Alonso AA, Hasselmo ME. 2002. Simulations of the role of the muscarinic-activated calcium-sensitive nonspecific cation current INCM in entorhinal neuronal activity during delayed matching tasks. *J Neurosci* **22:** 1081–1097.

Fujisawa S, Amarasingham A, Harrison MT, Buzsaki G. 2008. Behavior-dependent short-term assembly dynamics in the medial prefrontal cortex. *Nat Neurosci* **11:** 823–833.

Fuster JM. 1973. Unit activity in prefrontal cortex during delayed-response performance: Neuronal correlates of transient memory. *J Neurophysiol* **36:** 61–78.

Hafting T, Fyhn M, Molden S, Moser MB, Moser EI. 2005. Microstructure of a spatial map in the entorhinal cortex. *Nature* **436:** 801–806.

Hasselmo ME, Stern CE. 2006. Mechanisms underlying working memory for novel information. *Trends Cogn Sci* **10:** 487–493.

Huang Y, Brandon MP, Griffin AL, Hasselmo ME, Eden UT. 2009. Decoding movement trajectories through a T-maze using point process filters applied to place field data from rat hippocampal region CA1. *Neural Comput* **21:** 3305–3334.

Jensen O, Lisman JE. 1996. Novel lists of $7+/-2$ known items can be reliably stored in an oscillatory short-term memory network: Interaction with long-term memory. *Learn Mem* **3:** 257–263.

Jensen O, Lisman JE. 2005. Hippocampal sequence-encoding driven by a cortical multi-item working memory buffer. *Trends Neurosci* **28:** 67–72.

Johnson A, Redish AD. 2007. Neural ensembles in CA3 transiently encode paths forward of the animal at a decision point. *J Neurosci* **27:** 12176–12189.

Klink R, Alonso A. 1997. Muscarinic modulation of the oscillatory and repetitive firing properties of entorhinal cortex layer II neurons. *J Neurophysiol* **77:** 1813–1828.

Koene RA, Gorchetchnikov A, Cannon RC, Hasselmo ME. 2003. Modeling goal-directed spatial navigation in the rat based on physiological data from the hippocampal formation. *Neural Netw* **16:** 577–584.

Komorowski RW, Manns JR, Eichenbaum H. 2009. Robust conjunctive item-place coding by hippocampal neurons parallels learning what happens where. *J Neurosci* **29:** 9918–9929.

Lipton PA, White JA, Eichenbaum H. 2007. Disambiguation of overlapping experiences by neurons in the medial entorhinal cortex. *J Neurosci* **27:** 5787–5795.

Lisman JE, Idiart MA. 1995. Storage of $7 +/- 2$ short-term memories in oscillatory subcycles. *Science* **267:** 1512–1515.

McGaughy J, Koene RA, Eichenbaum H, Hasselmo ME. 2005. Cholinergic deafferentation of the entorhinal cortex in rats impairs encoding of novel but not familiar stimuli in a delayed nonmatch-to-sample task. *J Neurosci* **25:** 10273–10281.

McNaughton BL, Barnes CA, O'Keefe J. 1983. The contributions of position, direction, and velocity to single unit-activity in the hippocampus of freely-moving rats. *Exp Brain Res* **52:** 41–49.

Moser EI, Moser MB. 2008. A metric for space. *Hippocampus* **18:** 1142–1156.

O'Keefe J, Burgess N. 1996. Geometric determinants of the place fields of hippocampal neurons. *Nature* **381:** 425–428.

O'Keefe J, Burgess N, Donnett JG, Jeffery KJ, Maguire EA. 1998. Place cells, navigational accuracy, and the human hippocampus. *Philos Trans R Soc Lond B Biol Sci* **353:** 1333–1340.

Parikh V, Kozak R, Martinez V, Sarter M. 2007. Prefrontal acetylcholine release controls cue detection on multiple timescales. *Neuron* **56:** 141–154.

Quirk GJ, Muller RU, Kubie JL, Ranck JB Jr. 1992. The positional firing properties of medial entorhinal neurons: Description and comparison with hippocampal place cells. *J Neurosci* **12:** 1945–1963.

Sargolini F, Fyhn M, Hafting T, McNaughton BL, Witter MP, Moser MB, Moser EI. 2006. Conjunctive representation of position, direction, and velocity in entorhinal cortex. *Science* **312:** 758–762.

Schon K, Hasselmo ME, Lopresti ML, Tricarico MD, Stern CE. 2004. Persistence of parahippocampal representation in the absence of stimulus input enhances long-term encoding: A functional magnetic resonance imaging study of subsequent memory after a delayed match-to-sample task. *J Neurosci* **24:** 11088–11097.

Schon K, Atri A, Hasselmo ME, Tricarico MD, LoPresti ML, Stern CE. 2005. Scopolamine reduces persistent activity related to long-term encoding in the parahippocampal gyrus during delayed matching in humans. *J Neurosci* **25:** 9112–9123.

Schon K, Tinaz S, Somers DC, Stern CE. 2008. Delayed match to object or place: An event-related fMRI study of short-term stimulus maintenance and the role of stimulus pre-exposure. *Neuroimage* **39:** 857–872.

Sharp PE. 1996. Multiple spatial/behavioral correlates for cells in the rat postsubiculum: Multiple regression analysis and comparison to other hippocampal areas. *Cereb Cortex* **6:** 238–259.

Solstad T, Boccara CN, Kropff E, Moser MB, Moser EI. 2008. Representation of geometric borders in the entorhinal cortex. *Science* **322:** 1865–1868.

Stern CE, Sherman SJ, Kirchhoff BA, Hasselmo ME. 2001. Medial temporal and prefrontal contributions to working memory tasks with novel and familiar stimuli. *Hippocampus* **11:** 337–346.
Suzuki WA, Miller EK, Desimone R. 1997. Object and place memory in the macaque entorhinal cortex. *J Neurophysiol* **78:** 1062–1081.
van der Meer MA, Redish AD. 2009. Covert Expectation-of-Reward in Rat Ventral Striatum at Decision Points. *Front Integr Neurosci* **3:** 1.
van der Meer MA, Redish AD. 2010. Expectancies in decision making, reinforcement learning, and ventral striatum. *Front Neurosci* **4:** 6. doi: 10.3389/neuro.01.006.2010.
Wood ER, Dudchenko PA, Robitsek RJ, Eichenbaum H. 2000. Hippocampal neurons encode information about different types of memory episodes occurring in the same location. *Neuron* **27:** 623–633.
Yoshida M, Fransen E, Hasselmo ME. 2008. mGluR-dependent persistent firing in entorhinal cortex layer III neurons. *Eur J Neurosci* **28:** 1116–1126.
Young BJ, Otto T, Fox GD, Eichenbaum H. 1997. Memory representation within the parahippocampal region. *J Neurosci* **17:** 5183–5195.
Zhang K, Ginzburg I, McNaughton BL, Sejnowski TJ. 1998. Interpreting neuronal population activity by reconstruction: Unified framework with application to hippocampal place cells. *J Neurophysiol* **79:** 1017–1044.

Received February 6, 2012; accepted in revised form March 28, 2012.